

## Optimization of the inverted perovskite $\text{CH}_3\text{NH}_3\text{PbI}_3$ planar heterojunction for solar cells applications

M. Kemouche<sup>b</sup>, A. Aissat<sup>a,b,c,\*</sup>, S. Nacer<sup>b</sup>, S. Dupont<sup>c</sup>, J. P. Vilcot<sup>c</sup>

<sup>a</sup>University of Ahmed Draia, Adrar, Algeria

<sup>b</sup>LATSI Laboratory, Department of electronics, University Blida1, Blida, Algeria

<sup>c</sup>Institute of Electronics, Microelectronics and Nanotechnology (IEMN), UMR CNRS 8520, University of Sciences and Technologies of Lille 1, Avenue Poincare, 60069, 59652 Villeneuve of Ascq, France

The purpose of our paper is to simulate and optimize the electro-optical characteristics of a reversed Perovskite planar solar cell. Firstly, the synthesis of the  $\text{CH}_3\text{NH}_3\text{PbI}_3$  was exposed. Then, the absorption, reflection and transmission phenomena were studied. The effects of the thicknesses of  $\text{CH}_3\text{NH}_3\text{PbI}$  (d) and HTL (D) layers on the efficiency of the presented have been simulated. Subsequently, the back contact metals effect on  $J_{sc}$ ,  $V_{oc}$ , FF and  $\eta$  was taken into account. For a thickness  $d=0.6\mu\text{m}$ , the output parameters reached  $V_{oc}=1.07\text{V}$ ,  $J_{sc}=22.75\text{mA}/\text{cm}^2$ ,  $\text{FF}=78\%$  and  $\eta=19.02\%$ . Besides, the efficiency is reduced by the defect density at the  $\text{CH}_3\text{NH}_3\text{PbI}_3/\text{PEDOT:PSS}$  interface more than that at the  $\text{PCBM}/\text{CH}_3\text{NH}_3\text{PbI}_3$  interface and it should be less than  $10^{13}\text{ cm}^{-3}$  to have better solar cell performance.

(Received June 4, 2024; Accepted September 21, 2024)

*Keywords:* Materials, Perovskite, Defect density, Solar cell, Photovoltaic, Optoelectronics

### 1. Introduction

Gustav Rose introduced the Perovskites for the first time in 1839, and the Russian mineralogist Lew Alexeyewitsch Perovskite gave them their name [1]. Presented again in 2009 by Kojima et al. [2] and since then they have caused immense reflection from many research subjects in the photovoltaic field. Organic-inorganic metal halide photovoltaic have developed as a main candidate for the next generation thin photovoltaic technology or emerging photovoltaics. This is due to the brilliant efficiency, ease and low cost of the manufacturing process compared to other third generation thin film technology, especially: dye-sensitized, organic and quantum dot solar cells. These factors make them a promising technology for the future photovoltaic devices [3-11]. This interest concerns their remarkable physical and optical properties for example: the adaptable bandgap energy beginning 1.5 eV at 2.4 eV [11], a broad absorption range that matches the solar spectrum [12], a strong absorption coefficient, high  $V_{oc}$  about 1.30 V with long electron diffusion length of 100nm [9,11]. The optoelectronic characteristics of Perovskite material are greatly varied by the crystal structure. Generally, Perovskites constitute a class of crystalline compounds that acquire simple cubic crystalline structure having a chemical formula as  $\text{ABX}_3$ , [1,13,14]. Where A represents the organic cation ( $\text{A} = \text{CH}_3\text{NH}_3^+$  or  $\text{NH}_2\text{CH}_3\text{NH}_2^+$ ), B named the inorganic metal cation ( $\text{B}=\text{Pb}^{2+}$ ,  $\text{Sn}^{2+}$ ,  $\text{Ge}^{2+}$ ) with X representing the halogen ion ( $\text{X}=\text{I}$ ,  $\text{Br}$ ,  $\text{Cl}$ ) [6, 8-11, 15]. Over the past fifteen years, several researches have attempted to augment the efficiency. Other researchers have used mixture lead halide compounds  $\text{CH}_3\text{NH}_3\text{PbX}$  ( $\text{X} = \text{Br}$  and  $\text{I}$ ) as visible light absorber for photovoltaics, and have had efficiencies of 3.81% for  $\text{X} = \text{Br}$  and 3.13% for  $\text{X} = \text{I}$  [2]. This value has been enhanced several times, a value of 25.2% was found [16], while very recently [17], for  $\alpha$ -FAPbI<sub>3</sub> based Perovskite solar cells, have exceeded this value where the recorded PCE was 25.6%. The efficiency can exceed the second-generation commercialized ones for example: solar cells made of CdTe and CIGS materials which have a record efficiency about 22.90%. [18].

---

\* Corresponding author: sakre23@yahoo.fr  
<https://doi.org/10.15251/JOR.2024.205.667>

The Perovskite solar cells (PSCs) have other advantages suitable for photovoltaic conversion like: flexibility, semi-transparency and light-weight. Among the most commonly used Perovskite absorbers, for example: there are methylammonium lead iodide ( $\text{MAPbI}_3$ ) and formamidinium lead iodide ( $\text{FAPbI}_3$ -1.48eV) [19]. However, organic inorganic metal halides Perovskite are being studied for other applications; in transistor and Light Emitting Diode (LED) technology, due to their crucial optoelectronic characteristics and the solution process ability of these semiconductors [20]. In addition, Perovskite materials are especially attached as the top solar cell in the tandem solar cell. The basic solar cell can produce of c-Si or CIGS [21]. The p-i-n reversed Perovskite solar cell is extensively used because of the fabrication process as a low down temperature solution [21, 22].

In this paper, we have represented the synthesis of Perovskite ( $\text{CH}_3\text{NH}_3\text{PbI}_3$ ) generated on the technique used by [23,24]. We have studied the optical parameters of the Perovskite absorber such as absorption, reflection and transmission coefficients. The complex refractive index derived from the experimental work of P. Löper *et al* [24] has been used. Then the thickness of Perovskite absorption, HTL thickness and using different metal back contacts consequence on the solar cells electrical parameters was studied. In addition, the influence of effective state density  $N_c$  and  $N_v$  on  $V_{oc}$  and PCE was considered. Also, the defect density at the  $\text{CH}_3\text{NH}_3\text{PbI}_3/\text{PEDOT:PSS}$  and  $\text{PCBM}/\text{CH}_3\text{NH}_3\text{PbI}_3$  interface effect on the efficiency has been presented. The energy levels of the  $\text{CH}_3\text{NH}_3\text{PbI}_3$  shell, the Highest Occupied Molecular Orbital (HOMO) Lowest Unoccupied Molecular Orbital (LUMO) are 5.4 and 3.9eV in that order. These levels coincide with the energy levels of the fullerene PCBM (phenyl-C61-butyric acid methyl ester) (HOMO: 5.9 and LUMO: 3.9 eV). Under illumination, photodissociation of the exciton is at the interface. The electron passes to the LUMO level of the PCBM then collected at the cathode, at the same time the holes can be transferred to the HOMO level of PEDOT: PSS (Poly (3,4-ethylenedioxythiophene): poly (styrene sulfonate) and collected at the anode [25,26]. The simulation has been completed at AM 1.5G, room temperature and  $\phi=1000\text{W}/\text{m}^2$ . Figure 1 presents the different layers of the solar cell studied.

## 2. Theoretical model

The synthesis technique of E.S.Yudanova *et al.*[22] and Y. Dang *et al.* [23] of  $\text{CH}_3\text{NH}_3\text{PbI}_3$  consists of synthesis of methylamine iodide ( $\text{CH}_3\text{NH}_3\text{I}$ ) and synthesis of  $\text{PbI}_2$  Methylammoniumiodide was resulted by [23,24]. The refraction coefficient was measured experimentally by P. Löper *et al* [24]. The absorption coefficient can be calculated by [27]. We observe that  $\text{CH}_3\text{NH}_3\text{PbI}_3$  has  $\alpha = 5.10^5\text{cm}^{-1}$ , and contains a wide absorption range beginning UV (350 nm) to PI (800 nm). The  $\text{CH}_3\text{NH}_3\text{PbI}_3$  material has two absorption peaks: 760 and 480 nm, in that order. The peak corresponding to 760 nm represents the direct bandgap energy for recombination from the valance band (BV) to the conduction band (BC) which is 1.64eV. The second peak 480 nm is tuned to the direct recombination starting BV to BC which is around 2.58 eV [9, 28-31]. The reflection is calculated by using the relation [25,29,32].

For the transmission spectrum, there are three regions. The first is for wavelengths less than 540nm, the transmission is almost zero due to high absorption in this region [3]. The second is divided into two parts, one for wavelengths between 540 and 730 nm the transmission increases to 23%, the other part is for wavelengths ranging from 730 to 800nm where the transmission increases very quickly to achieve 64%. The third region corresponds to wavelengths greater than 800nm, where wavelengths increase slowly compared to the last region. The maximum transmission level is 69%, obtained for a wavelength of about 900 nm. These acquired results are extremely agreement with the empirical results [32-34]. The transmission can be determined as follow [27]. In the study we used the SCAPS D1 software. Calculation parameters of the studied solar cell were carefully selected from practical and theoretical references, they are given in Table 1 [35-40]. The calculations are accomplished on the resolution of the Poisson and continuity equations implemented [36,41]. The transfer of charge carriers by derivation and diffusion is proposed [11,36].

Table. 1. Material parameters used in our simulation are listed as follows.

Parameter	HTL (PEDOT: PSS)	ETL (PCBM)	CH <sub>3</sub> NH <sub>3</sub> PbI <sub>3</sub>
d(μm)	0.20	0.20	0.30
E <sub>g</sub> (eV)	2.20	2.00	1.55
ε <sub>r</sub>	3.00	3.90	6.50
N <sub>c</sub> (cm <sup>-3</sup> )	1.10 <sup>21</sup>	2.5.10 <sup>21</sup>	2.2.10 <sup>18</sup>
N <sub>v</sub> (cm <sup>-3</sup> )	1.10 <sup>21</sup>	2.5.10 <sup>21</sup>	1.8.10 <sup>19</sup>
μ <sub>n</sub> (cm <sup>2</sup> /Vs)	1	0.20	10
μ <sub>p</sub> (cm <sup>2</sup> /Vs)	40	0.20	10
N <sub>d</sub> (cm <sup>-3</sup> )	-	2.93.10 <sup>17</sup>	5.3.10 <sup>9</sup>
N <sub>a</sub> (cm <sup>-3</sup> )	1.10 <sup>19</sup>	-	-
N <sub>t</sub> (cm <sup>-3</sup> )	1.10 <sup>15</sup>	1.10 <sup>15</sup>	1.10 <sup>15</sup>

### 3. Results and discussion

The reversed CH<sub>3</sub>NH<sub>3</sub>PbI<sub>3</sub> has been defined: ITO/PEDOT: PSS/CH<sub>3</sub>NH<sub>3</sub>PbI<sub>3</sub>/PCBM/Au sandwiched between ITO and (Au) forming the transparent anode and cathode, respectively has been presented in figure 1. We have used PEDOT: PSS as hole transport layer (HTL) p-type is widely used in the inverse structure due to its high transparency and compatibility with the Perovskite [42, 43]. The Perovskite absorber layer CH<sub>3</sub>NH<sub>3</sub>PbI<sub>3</sub> is the intrinsic region. We used PCBM as electron transport layer (ETL) n-type instead of TiO<sub>2</sub> because of two factors: the PCBM has a conductivity of 0.016 mScm<sup>-1</sup> compared to 6x10<sup>-5</sup> mScm<sup>-1</sup> for TiO<sub>2</sub>, and the electron extraction from CH<sub>3</sub>NH<sub>3</sub>PbI<sub>3</sub> to PCBM is more important than in the case of TiO<sub>2</sub>[10]. When the cell is under illumination, there is a formation of the exciton in the Perovskite region [15]. Exciton dissociation will occur at the interface between ETL/Perovskite and HTL/Perovskite; free charge carriers will move towards the electrodes.

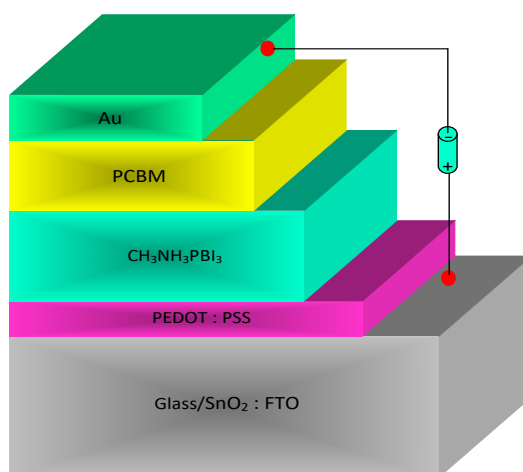


Fig. 1. Structure of CH<sub>3</sub>NH<sub>3</sub>PbI<sub>3</sub> solar cell.

The variation of the absorption coefficient ( $\alpha$ ) of CH<sub>3</sub>NH<sub>3</sub>PbI<sub>3</sub> vs of wavelength ( $\lambda$ ) have been shown in Figure 2. We note that the absorption region of the structure varies from 300 to 800 nm. In the region of 300 to 700 nm, the absorption coefficient varies from  $5.52 \times 10^5$  to  $0.35 \times 10^5$  cm<sup>-1</sup>. Then, the absorption coefficient continues to degrade until the wavelength of 800 nm becomes zero. Thus, the material CH<sub>3</sub>NH<sub>3</sub>PbI<sub>3</sub> is a very good absorber, especially around  $\lambda=300$  nm.

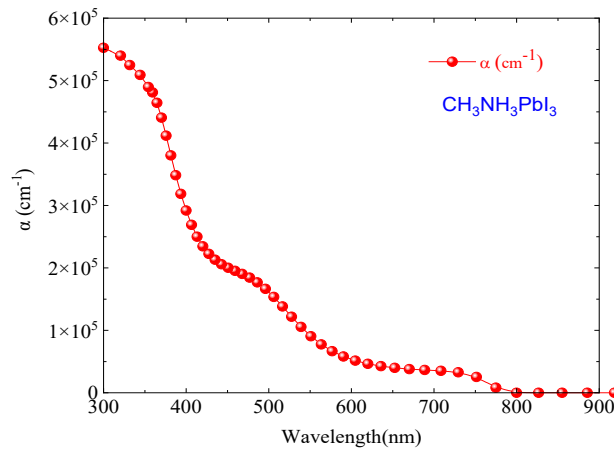


Fig. 2.  $\alpha$  evolution of the  $\text{CH}_3\text{NH}_3\text{PbI}_3$  vs wavelength.

The evolution of the reflection and transmission coefficients of the absorbing layer  $\text{CH}_3\text{NH}_3\text{PbI}_3$  as a function of the  $\lambda$  was studied. This simulation shows us an idea to optimize the two coefficients R and T in order to improve  $\alpha$  coefficient in addition to the solar cell efficiency. The influence of the variation in the absorber thickness ( $d$ ) and HTL film ( $D$ ) was studied in the following part. The energy diagram of the inverse p-i-n structure at equilibrium is exposed in Figure 4. An energy barrier of 1.70 eV is present between LUMO of HTL and  $\text{CH}_3\text{NH}_3\text{PbI}_3$ . The  $\text{CH}_3\text{NH}_3\text{PbI}_3$  layer prevents the movement of photoelectrons that move from  $\text{CH}_3\text{NH}_3\text{PbI}_3$  to the HTL layer. In addition, the 0.50eV energy barrier existing between the HOMO levels of  $\text{CH}_3\text{NH}_3\text{PbI}_3$  and the PCBM is able to prevent holes from moving to the PCBM layer (ETL). The existence of these barriers improves the component efficiency.

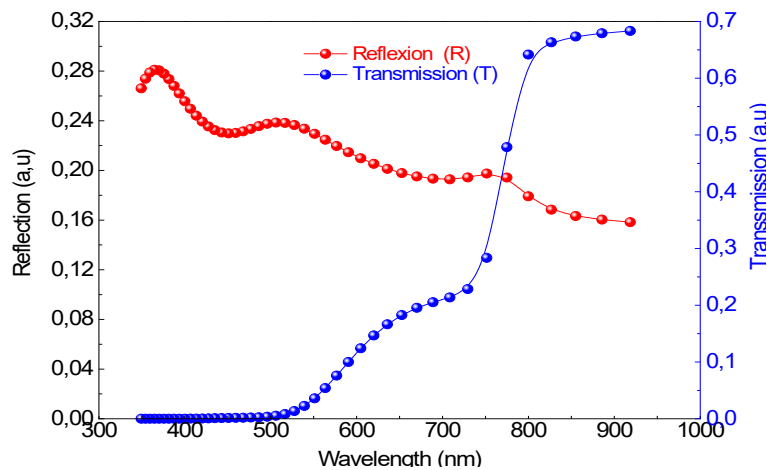


Fig. 3. wavelength impact on the reflection and transmission coefficients of  $\text{CH}_3\text{NH}_3\text{PbI}_3$ .

Figure. 5 exposes the influence of  $\lambda$  and  $d$  on the external quantum efficiency (EQE). We can see that the absorption range varies between 300 to 800nm, with EQE amplitude which reaches 90%. Another phenomenon can be observed is that; when the thickness  $d$  varies from 200 to 800nm, the amplitude increases considerably. When the thickness of the structure  $d$  changes from 200 to 800nm and the wavelength  $\lambda$  equal 600nm the amplitude of EQE varies from 71.95% to 89.87% respectively. The  $d$  of the optimal  $\text{CH}_3\text{NH}_3\text{PbI}_3$  absorbing layer is around 600nm [34,44-46]. Then, the amplitude of the EQE becomes zero in the  $\lambda$  range above 800 nm, which is in good accord with the  $\alpha$  curve (Figure 2).

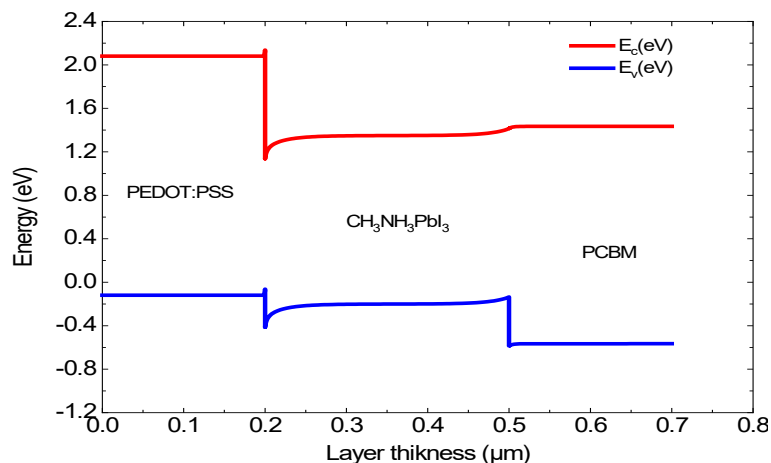


Fig. 4. Band energy diagram of simulated solar cell structure.

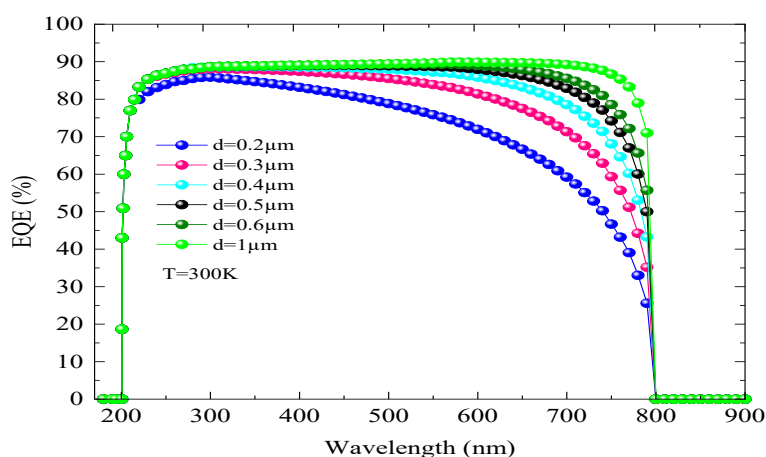


Fig. 5. Variation of EQE vs wavelength of simulated solar cell for different thickness.

The J-V variation for different thickness  $d$  is shown in Figure. 6. The thickness  $d$  influence on the  $\text{CH}_3\text{NH}_3\text{PbI}_3$  film was reported. When the thickness  $d$  increases from 0.2 to  $1\mu\text{m}$ , the current density ( $J_{\text{sc}}$ ) improves, however the open circuit voltage ( $V_{\text{oc}}$ ) decreases. The thickness  $d$  impact on  $J_{\text{sc}}$  is more considerable than alone on  $V_{\text{oc}}$ . Then, for the thickness  $d=600\text{nm}$ , the  $J_{\text{sc}}$  and  $V_{\text{oc}}$  parameters exceed  $22\text{mA}/\text{cm}^2$  and  $1.05\text{V}$  respectively. We detect that when the  $d$  increases since 200 to  $1000\text{nm}$ , we had a gain in  $\Delta J_{\text{sc}}=4.8\text{mA}/\text{cm}^2$  and a loss in  $\Delta V_{\text{oc}}=0.08\text{V}$ . Figure. 7 illustrates the influence of  $D$  and  $d$  on the output parameters ( $J_{\text{sc}}$ ,  $V_{\text{oc}}$ , FF, and  $\eta$ ). Figure. 7.a represents the variation of the ( $J_{\text{sc}}$ ) vs of the  $D$  and  $d$  at room temperature. The short circuit density exceeds  $23\text{mA}/\text{cm}^2$ . This study allows us to optimize the  $d$  and  $D$  in order to maximize a  $J_{\text{sc}}$ .

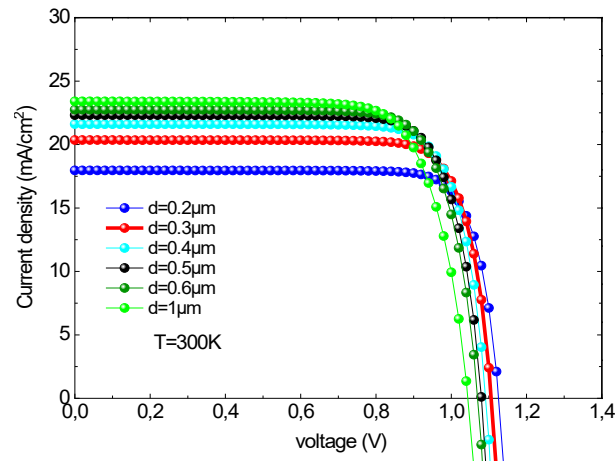


Fig. 6. J-V characteristic for different thicknesses ( $d$ ).

The thicknesses  $d$  and  $D$  effect on the  $V_{oc}$  is presented in figure. 7.b. Our simulation results show that the  $V_{oc}$  voltage varies between 1.04 to 1.15V. We can optimize the thicknesses  $d$  and  $D$  to create an efficient and reliable solar cell. The  $V_{oc}$  parameter has been found to decrease with increasing the active layer thickness. For a small Perovskite thickness of 100nm, the charge extraction is large according to the high value of  $V_{oc}=1.15V$  which indicates a weak recombination due to the diffusion width, which is greater than the absorber thickness  $d$ . [11, 45-47].

The  $V_{oc}$  reduction is due to the increase in thickness  $d$  and the reducing in bandgap energy [48]. We report that the charge carriers diffusion length is shorter than  $d$ , so the charge carriers will be recombined in the absorbing layer [45].

Figure.7.c represents the impact of thicknesses  $d$  and  $D$  on the form factor (FF) at  $T=300K$ . When the thicknesses  $d$  and  $D$  vary from 100 to 800nm and 50 to 200nm, respectively, the parameter FF changes from 70.75 to 83.58%. When the thickness  $d$  varies in the range 100-200 nm and  $D$  varies in the range 50-200nm the FF parameter is around 83%. These results allow us to choose the couples ( $d$  and  $D$ ) to create a high performance and very reliable solar cell.

The thicknesses  $d$  and  $D$  impact on the solar cell performances at  $T=300K$  is given away in Figure. 7. d. When the thicknesses ( $d$  and  $D$ ) vary from 100 to 800nm and 50 to 200nm, respectively, we note that the efficiency varies from 12.42 to 19.04%. This study allows us to improve the solar cell performances, also to minor recombination and device resistance, it's crucial to decrease the HTML thickness [11,45, 49,50]. By virtue of our study, we can deduce that the solar cell structure optimizes and corresponds at  $d= 600$  nm and  $D= 50$ nm with  $J_{sc}=22.78\text{mA}/\text{cm}^2$ ,  $V_{oc}= 1.07V$ ,  $FF=77.98\%$  and  $\eta=19.02\%$ . Our results obtain are in concord with the literature results [11,45]. Table. 2 shows the couples ( $d$ ,  $D$ ) impact on the  $V_{oc}$ ,  $J_{sc}$ , FF and  $\eta$ . These results allow us to produce a more efficient and reliable solar cell. We notice that the best thicknesses  $d$  and  $D$  are 600 and 50nm respectively with efficiency equal 19.02%.

Table. 2. The  $d$  and  $D$  thicknesses impact on the  $J_{sc}$ ,  $V_{oc}$ , FF and  $\eta$ .

( $d,D$ ) nm	$J_{sc}(\text{mA}/\text{cm}^2)$	$V_{oc}(V)$	FF(%)	$\eta(\%)$
(200, 50)	17.95	1.12	81.88	16.57
(200,200)	17.91	1.12	81.89	16.54
(600,50)	22.78	1.07	77.99	19.02
(600,200)	22.75	1.07	77.95	18.98
(800,50)	23.24	1.06	76.78	18.83
(800, 200)	23.19	1.06	76.76	18.80

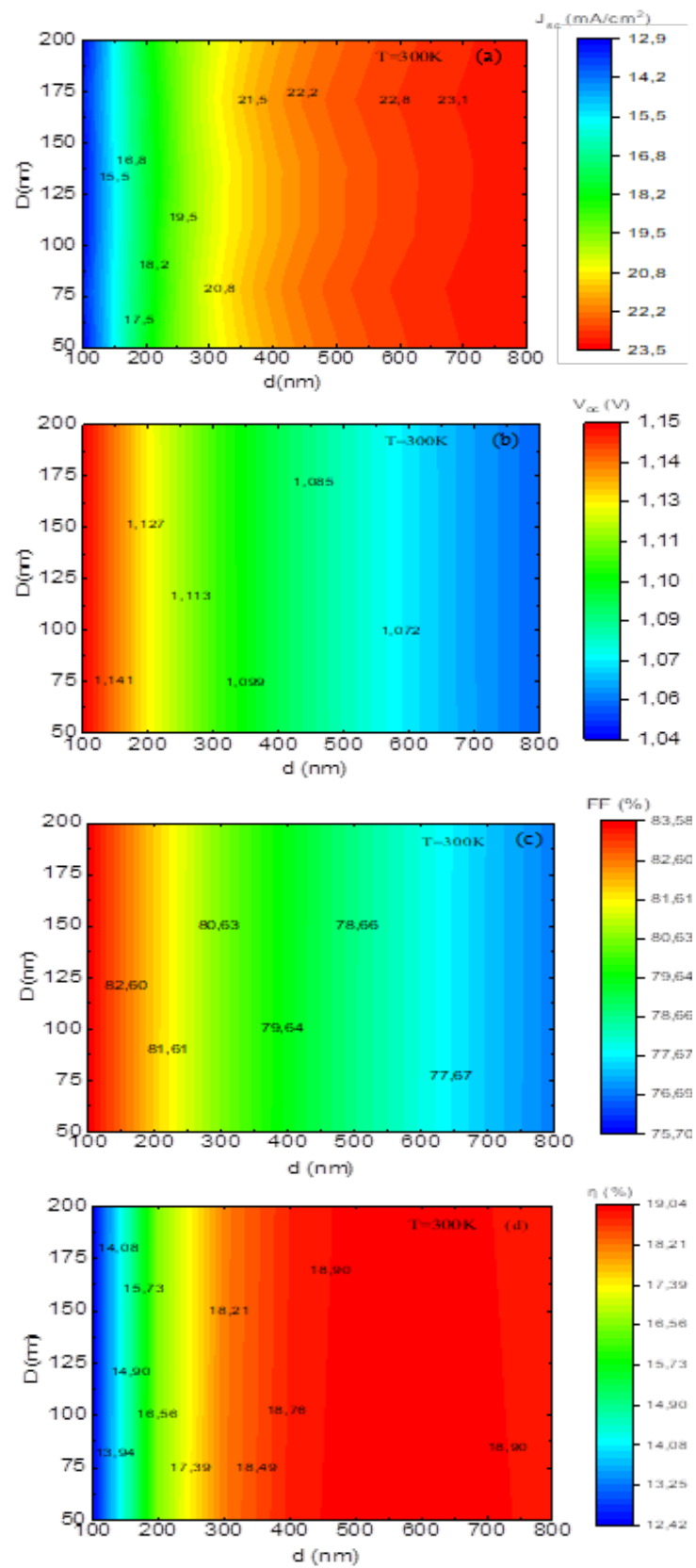


Fig. 7. a) Thickness  $d$  and  $D$  impact on  $J_{sc}$ , b) thickness  $d$  and  $D$  impact  $V_{oc}$ , c) thickness  $d$  and  $D$  impact on FF, d) thickness  $d$  and  $D$  impact on  $\eta$  %.

The optimized J-V characteristic curve is validated with the experimental results obtained by [10,43] (Figure 8). For equal  $0.3 \mu\text{m}$ , the simulation shows a significant conversion efficiency of 18.15%. We find that our results converge towards the experimental of J.H. Héo et al. [10] and S. Rai et al. [43]. Furthermore, 19.02% efficiency was obtained using thickness  $d=600 \text{ nm}$  for  $\text{CH}_3\text{NH}_3\text{PbI}_3$  and  $D=50 \text{ nm}$  for HTL with ETL thickness fixed at  $200 \text{ nm}$ . Table. 3 illustrates the comparison between the results obtained compared to other works in the literature [10, 22,43, 49,50]. In order to explain the diverse output work ( $\Phi$ ) of the metallic back contact influence on the efficiency, a simulation has been presented which involves the study of this phenomenon. For this, we used several materials such as: Silver Ag, Aluminum Al, Tin Sn, Copper Cu and Iron Fe, or Au [51].

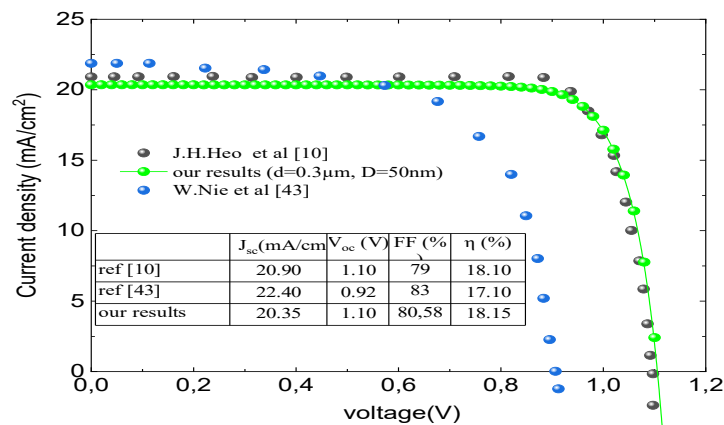


Fig. 8. J-V comparison of optimized and experimental J-V characteristic [10,43].

Table. 3. Comparative table including our structure and results of some published references.

Structure	$V_{oc}$ (V)	$J_{sc}$ (mA /cm <sup>2</sup> )	FF(%)	$\eta$ (%)
ITO/NiO/CH <sub>3</sub> NH <sub>3</sub> PbI <sub>3-x</sub> Cl <sub>x</sub> /PCBM./Ag[17]	1.06	21.02	74	16.48
ITO/PEDOT: PSS /CH <sub>3</sub> NH <sub>3</sub> PbI <sub>3</sub> /PCBM/Au[7]	1.10	20.90	79	18.10
FTO/PEDOT: PSS /CH <sub>3</sub> NH <sub>3</sub> PbI <sub>3</sub> /PCBM/Al[38]	0.92	22.40	83	17.10
ITO/PEDOT: PSS /CH <sub>3</sub> NH <sub>3</sub> PbI <sub>3</sub> /PC <sub>61</sub> BM/Al[44]	0.89	18.85	80	13.37
FTO: SnO <sub>2</sub> /PEDOT: PSS/CH <sub>3</sub> NH <sub>3</sub> PbI <sub>3</sub> /PCBM./Al[45]	0.97	18.22	76.77	13.51
ITO/PEDOT: PSS/CH <sub>3</sub> NH <sub>3</sub> PbI <sub>3</sub> /PCBM/Au [our work]	1.07	22.75	78	19.02

In Figure. 9. the metallic back contacts Au, Al, Ag, Sn, Cu and Fe effect on the J-V was studied and analyzed. We find that gold (Au), silver (Ag), and aluminum (Al) contacts have better performance than tin (Sn), copper (Cu), and iron (Fe) contacts. The parameters  $J_{sc}$ ,  $V_{oc}$ , FF and  $\eta$  are equal  $20.35 \text{ mA/cm}^2$ ,  $1.11 \text{ V}$ ,  $80.60\%$  and  $18.15\%$  respectively with  $d=0.6 \mu\text{m}$ . Table. 4 presents the inverted Perovskite solar cell parameters for Au, Ag, Al, Sn, Cu, and Fe metallic back contacts. We report that as the metal work function increases from Ag to Fe, the  $V_{oc}$  and FF parameters decrease from  $1.11$  to  $1.05 \text{ V}$  and  $80.58$  to  $61.27\%$ , respectively, while the PCE decreases from  $18.15$  to  $13.16\%$  [52]. This event is caused by the augmentation of the energy between the CB of the PCBM and the metal Fermi level. When the metal has a low  $\Phi$ , the Schottky barrier prevents the holes transfer from the BV of  $\text{CH}_3\text{NH}_3\text{PbI}_3$  to the metal and the photogenerated electrons can be transferred from the CB of the  $\text{CH}_3\text{NH}_3\text{PbI}_3$  to the electrode (Ag).

Table. 4. Inverted Perovskite solar cell parameters of for different metal back contact work function with  $d=0.3\mu\text{m}$ ,  $D=50\text{nm}$ .

Metal	$\Phi(\text{eV})$	$V_{oc}(\text{V})$	$J_{sc}(\text{mA}/\text{cm}^2)$	FF(%)	$\eta(\%)$
Au	5.10	1.11	20.35	80.60	18.15
Ag	4.26	1.11	20.35	80.58	18.15
Al	4.30	1.11	20.35	80.57	18.14
Sn	4.42	1.11	20.35	79.65	17.94
Cu	4.65	1.09	20.34	63.63	14.10
Fe	4.70	1.05	20.34	61.28	13.16

However, the  $\phi$  of the Ag is inferior to that of Fe alone; the Schottky barrier prevents the electrons transport as of the Perovskite to the metal, which decreases the solar cell efficiency. When the metal has a high work function like Au (5.1 eV), the electrode can capture both photogenerated electrons and holes [ 51], consequently, these performances are internalizing. For copper and iron, they have S-shaped curves (J-V), this is due to the large barrier between the PCBM and the back contact. So, the injection of electrons to the back contact is able to prevent [51]. We note that when using Cu and Fe contacts the FF reaches 63.50 and 61%, respectively. On the other hand, if we use the Ag, Al and Ag the FF reaches 80.60, 80.55 and 80.60%, respectively. The increasing in series resistance  $R_s$  causes the FF improvement.

These phenomena can be attributed to the insertion of Cu atoms into the material of the ETM layer, we are able to expect the same phenomena for iron Fe. Our simulation results are very adjacent to the results obtained by Behrouz Nejad et al. [50]. To choose the best electrodes to use in our simulation: Au, Ag or Al, we must take into account the phenomenon of stability of the metal because their photovoltaic performances are almost the same. To study the effect of CB and VB state densities on  $V_{oc}$  and  $\eta$ , we varied the  $N_c$  and  $N_v$  densities from  $1 \times 10^{17}$  to  $1 \times 10^{19} \text{cm}^{-3}$ .

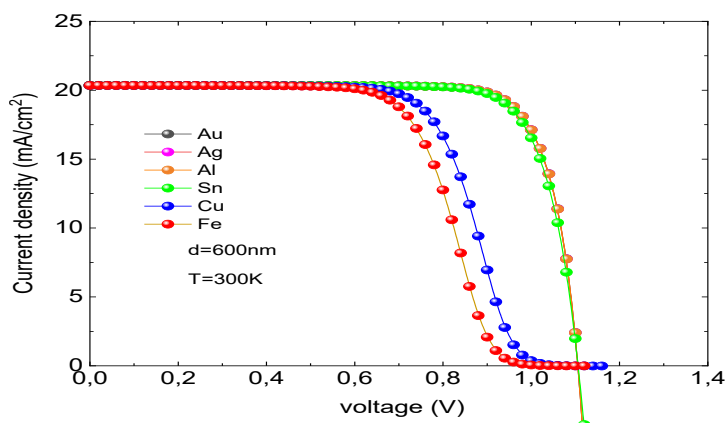


Fig. 9. Impact of different back contact metals on J-V characteristics.

In Figure. 10 the interface defect density ( $N_{Di}$ ) at the  $\text{CH}_3\text{NH}_3\text{PbI}_3/\text{PEDOT:PSS}$  effect on the characteristic J-V has been studied. The defects density at the interface was varied from  $10^{10}$  to  $10^{18} \text{cm}^{-3}$ . We note that growing the interface defects density degrades the J-V. Also, increasing the interface defects density decreases  $J_{sc}$ ,  $V_{oc}$ , FF and  $\eta$ . The optimal  $J_{sc}$  and  $V_{oc}$  parameters reached  $22.79 \text{mA}/\text{cm}^2$ ,  $1.07 \text{V}$ , respectively, with a defect density of  $10^{10} \text{cm}^{-2}$ . When, the density of interface defects increases from  $10^{10}$  to  $10^{18} \text{cm}^{-2}$ , the density  $J_{sc}$  and the voltage  $V_{oc}$  degrade by  $2.45 \text{mA}/\text{cm}^2$  and  $0.32 \text{V}$ , respectively. The decrease in  $J_{sc}$  is due to the interface defects density which is associated to the total lifetime of the recombination and the diffusion length [53-

56]. The decrease of  $V_{oc}$  depends of the enhancing of the  $N_{Di}$ ; this is owing to the position of the Fermi level, which will be in the medium of the bandgap energy of the Perovskite layer [57,58].

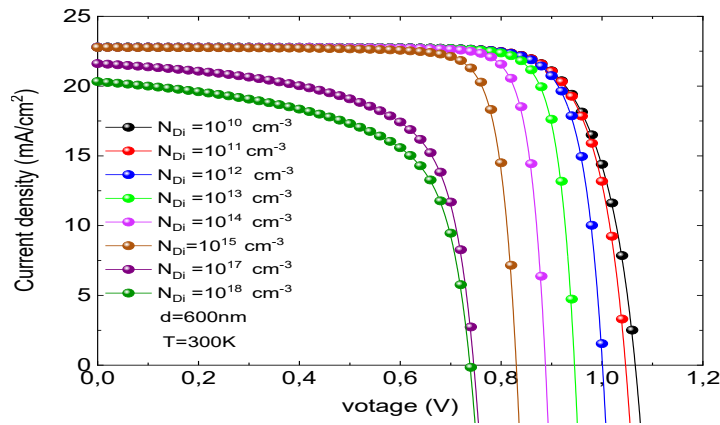


Fig. 10. Influence of interface defect density ( $N_{Di}$ ) in Perovskite/PEDOT: PSS on J-V characteristics.

In Figure. 11 the  $N_{Di}$  at the PCBM/ $CH_3NH_3PbI_3$  impact on the J-V has been taken into account. We note that the  $J_{sc}$  density is not influenced by the variation of the  $N_{Di}$ . In contrast, the increase in the  $N_{Di}$  induces a degradation of  $V_{oc}$ . When the  $N_{Di}$  varies from  $10^{10}$  to  $10^{18}cm^{-3}$  the voltage  $V_{oc}$  decreases of 0.08V. We reported that the  $N_{Di}$  at the  $CH_3NH_3PbI_3$ /PEDOT: PSS has a significant effect on the efficiency compared to the  $N_{Di}$  at the PCBM/ $CH_3NH_3PbI_3$ . This phenomenon occurs for the reason that in the solar cell, the released light is reversed. Also, in  $CH_3NH_3PbI_3$ /PEDOT: PSS the number of generated charge carrier electron-hole pairs is higher than that in PCBM/ $CH_3NH_3PbI_3$  interface. Then the recombination phenomenon is more important compared to PCBM/ $CH_3NH_3PbI_3$  interface [44,55,59,60].

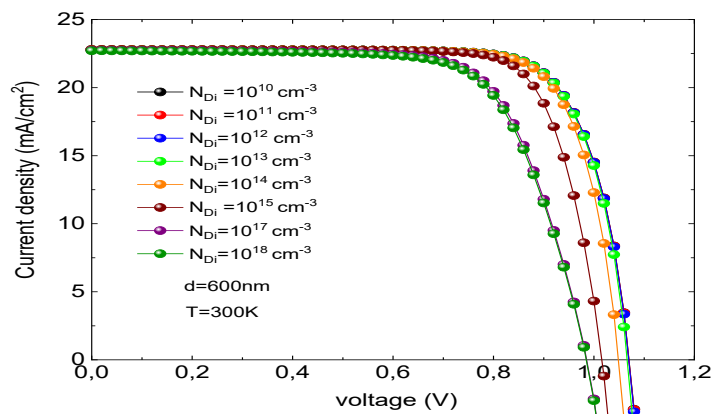


Fig. 11. Interface defect density ( $N_{Di}$ ) at Perovskite/PCBM effect on the J-V characteristic.

In figure. 12 the  $N_{Di}$  of  $CH_3NH_3PbI_3$ /PEDOT: PSS and PCBM/ $CH_3NH_3PbI_3$  interfaces impact on the efficiency was exposed. The red curve represents the  $N_{Di}$  of PCBM/ $CH_3NH_3PbI_3$  effect on the solar cell efficiency. In the region from  $10^{10}$  to  $10^{14}cm^{-3}$  the efficiency remains constant but when the  $N_{Di}$  exceeds  $10^{14}cm^{-3}$  the efficiency begins to decrease. For a change from  $10^{14}$  to  $10^{18}cm^{-3}$ , the increase decreases by 3.01%. The blue curve represents the  $N_{Di}$  of  $CH_3NH_3PbI_3$ /PEDOT effect on the solar cell efficiency. The results expose us that in the interval of  $10^{10}$  to  $10^{12}cm^{-3}$  the efficiency doesn't change, i.e. it isn't influenced by the interface

defect density, except beyond  $10^{12} \text{ cm}^{-3}$ , it decreases rapidly. When the  $N_{\text{Di}}$  of  $\text{CH}_3\text{NH}_3\text{PbI}_3/\text{PEDOT}$  varies of  $10^{12}$  to  $10^{18} \text{ cm}^{-3}$  the efficiency decreases until 9.52%.

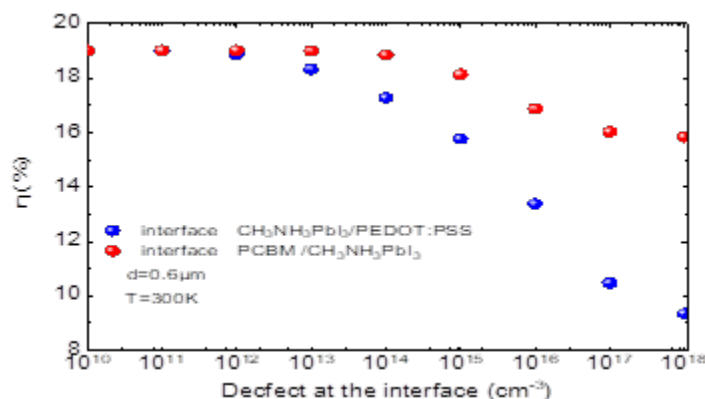


Fig. 12. Interface defect density effect on efficiency ( $\eta$ ).

#### 4. Conclusion

In this paper, the  $\text{CH}_3\text{NH}_3\text{PbI}_3$  Perovskite inverted planar solar cell was studied and enhanced. Firstly, we studied the optical parameters of  $\text{CH}_3\text{NH}_3\text{PbI}_3$  based Perovskite material, including absorption, reflection and transmittance. Then, the thicknesses  $d$  and  $D$  have been optimized. The best efficiency reaches 19.02% with  $d=0.6$  and  $D=0.3 \mu\text{m}$  respectively. The influence of different back contact metals on the solar cell efficiency was considered.

The best back contact is Au compared to other metals. When the defect density of both  $\text{CH}_3\text{NH}_3\text{PbI}_3/\text{PEDOT:PSS}$  and  $\text{PCBM}/\text{CH}_3\text{NH}_3\text{PbI}_3$  interfaces reaches  $1.10^{17} \text{ cm}^{-3}$ , the efficiency suffers losses of 2.99 and 8.55%, respectively. Moreover, the defect at the  $\text{CH}_3\text{NH}_3\text{PbI}_3/\text{PEDOT:PSS}$  interface affects the solar cell parameters more than the defect at the  $\text{PCBM}/\text{CH}_3\text{NH}_3\text{PbI}_3$  interface. In the perspective work we insert the Cl and Bi elements into the absorber material  $\text{CH}_3\text{NH}_3\text{PbI}_3$  sequentially to develop the stability and reliability of the solar cell.

#### References

- [1] F. Ünlü, E. Jung, S. Öz, H. Choi, T. Fischer, S. Mathur, *Materials, Processes, and Devices* (2021) 1-31; <https://doi.org/10.1002/9783527825790.ch1>.
- [2] A. Kojima, K. Teshima, Y. Shirai, T. Miyasaka, *J. Am. Chem. Soc.* 131(17) (2009) 6050-6051; <https://doi.org/10.1021/ja809598r>.
- [3] T.I. Mohammed, S.C.L. Koh, I.M. Reaney, A. Acquaye, G. Schileo, K.B. Mustapha, R. Greenough, *Perovskite solar cells*, *Renew. Sustain. Energy Rev.* 80 (2017) 1321–1344; <http://dx.doi.org/10.1016/j.rser.2017.05.095>
- [4] P. Gao, M. Grätzel, M.K. Nazeeruddin, *Energy Environ. Sci.* 7(8) (2014) 2448-2463. <https://doi.org/10.1039/C4EE00942H>
- [5] L. Et-taya, T. Ouslimane, A. Benami, *Solar Energy*. 201 (2020) 827–835 ; <https://doi.org/10.1016/j.solener.2020.03.070>.
- [6] M.A. Green, A.H. Baillie, H.J. Snaith, *J. Nature Photonics.* 8(7) (2014) 506-514; <https://doi.org/10.1038/nphoton.2014.134>.
- [7] Y. Ye, X. Run, X.H. Tao, H. Feng, X. Fei, W.L. Jun, *Chin. Phys.* (24)11 (2015) 116302; [https://doi: 10.1088/1674-1056/24/11/116302](https://doi:10.1088/1674-1056/24/11/116302)
- [8] T. Baikie, Y. Fang, J.M. Kadro, M. Schreyer, F. Wei, S.G. Mhaisalkar, M. Graetzel, T.J., *J. Mater. Chem. A.* 1(18) (2013) 5628-5641; <https://doi.org/10.1039/C3TA10518K>.

- [9] A. Yang, M. Bai, X. Bao, J. Wang, W. Zhang, J Nanomed, Nanotechnol. (2016) 7(5);[https://doi.org/ 10.4172/2157-7439.1000407](https://doi.org/10.4172/2157-7439.1000407).
- [10] J.H. Heo, H.J. Han, D. Kim, T.K. Ahn, S.H. Im, Sci.8(5) (2015) 1602-1608;<https://doi.org/10.1039/C5EE00120J>.
- [11] N. Rai, S. Rai, P.K. Singh, P. Lohia, D.K. Dwivedi, Journal of Materials Science, Materials in Electronics. (2020);<https://doi.org/10.1007/s10854-020-04175-z>.
- [12] S. De Wolf, J. Holovsky, S.J. Moon, P. Löper, B. Niesen, M. Ledinsky, F.J. Haug, J.H. Yum, C. Ballif, J. Phys. Chem. Lett, 5(6), (2014) 1035-1039;<https://doi.org/10.1021/jz500279b>.
- [13] P. Roy, N.K. Sinha, A. Khare, Woodhead Publishing, (2021) 239-257;  
<https://doi.org/10.1016/B978-0-12-819977-0.00011-1>
- [13] C.C. Vidyasagar, B.M.M. Flores, V.M.J. Pérez, Nano-Micro Lett. 10(4), (2018)1-34 ;  
<https://doi.org/10.1007/s40820-018-0221-5>.
- [14] J. Xiong, B. Yang, R. Wu, C. Cao, Y. Huang, C. Liu ,Z. Hu , H. Huang, Y. Gao, J. Yang, Organic Electronics. 24 (2015) 106–112; <https://doi.org/10.1016/j.orgel.2015.05.028>
- [15] S.W. Lee, S. Bae, D. Kim, H.S. Lee, Advanced Materials, 32(51) (2020) 2002202;  
<https://doi.org/10.1002/adma.202002202>
- [16] J. Jeong, M. Kim, J. Seo, H. Lu, P. Ahlawat, A. Mishra, Y. Yang, M.A. Hope, F.T. Eickemeyer, M. Kim, Y. Jin Yoon, I.W. Choi, B.P. Darwich, S. Ju Choi, Y. Jo, J. Hee Lee, B. Walker, S.M. Zakeeruddin, L. Emsley, U. Rothlisberger, A. Hagfeldt, D.S. Kim, M. Grätzel, J.Y. Kim, Nature, 592(7854) (2021) 381-385;<https://doi.org/10.1038/s41586-021-03406-5>
- [17] T. Kato , J.L. Wu , Y. Hirai, H. Sugimoto, V. Bermudez, Journals & Magazines, IEEE Journal of Photovoltaics, Volume: 9 Issue: 1(2018) 1-6;<https://doi.org/10.48103/jjeci12018/>
- [18] S. Karthick, S. Velumani, J. Bouclé, Solar Energy. 205 (2020) 349–357.<https://doi.org/10.1016/j.solener.2020.05.041>
- [19] K. Lin, J. Xing, L.N. Quan, F.P.G. Arquer, X. Gong, J. Lu, L. Xie, W. Zhao, D. Zhang, C. Yan, W. Li, X. Liu, Y. Lu, J. Kirman, E.H. Sargent, Q. Xiong, Z. Wei, Nature 562 (2018) 245-248; <https://doi.org/10.1038/s41586-018-0575-3>
- [20] R. K. Kothandaraman, Y. Jiang, T. Feurer, A. N. Tiwari, F. Fu, Wiley Small Methods 4(10) (2020) 1-56;<https://doi.org/10.1002/smt.202000395>
- [21] P. Zhao, Z. Liu, Z. Lin, D. Chen, J. Su, C. Zhang, J. Zhang, J. Chang, Y. Hao, Solar Energy. 169 (2018) 11–18; <https://doi.org/10.1016/j.solener.2018.04.027>
- [22] E.S. Yudanova, T.A. Duda, O.E. Tereshchenko, O.I. Semenova, Journal of Structural Chemistry, 58(8) (2017) 1567–1572; <https://doi.org/10.1134/S0022476617080133>
- [23] Y. Dang, Y. Liu, Y. Sun, D. Yuan, X. Liu, W. Lu, G. Liu, H. Xia, X. Tao, Cryst. Eng. Comm. 17(3)(2015) 665-670;<https://doi.org/10.1039/C4CE02106A>.
- [24] P. Löper, M. Stuckelberger, B. Niesen, J. Werner, M. Filipič, S.J. Moon, J.H. Yum, M. Topič, S.D. Wolf, C. Ballif, Journal of Physical Chemistry Letters, 6(1) (2014) 66–71;<https://doi.org/10.1021/jz502471h>
- [25] L. Meng, J. You, T.F. Guo, Y. Yang, Accounts of Chemical Research 49(1) 3 (2015).155-165; <https://doi.org/10.1021/acs.accounts.5b00404>
- [26] M. Fox, Solids-Optical properties. Title. II. Series. Oxford university press, QC176.8 06 F69, 2001. 530
- [27] H.B. Kim, H. Choi, J. Jeong, S. Kim, B. Walker, S. Song, J. Y. Kim, Nanoscale. 6(2014) 6679-6683;<https://doi.org/10.1039/C4NR00130C>.
- [28] X. Ziang, L. Shifeng, Q. Laixiang, P. Shuping, W. Wei, Y. Yu, Y. Li, C. Zhijian, W. Shufeng, D. Honglin, Y. Minghui, G. G. Qin, Optical Materials Express, Vol. 5, Issue 1, 1 (2015) 29-43; <https://doi.org/10.1364/OME.5.000029>
- [29] G. Xing, N. Mathews, S. Sun, S. Lim, Y. Lam, M. Gratzel, T. C. Sum, Science (2013) 342-344;  
<https://doi.org/10.1126/science.1243167>
- [30] C.W. Chen, S.Y. Hsiao, C.Y. Chen, H.W. Kang, Z.Y. Huang, H.W. Lin, J. Mater. Chem. A. 3(2015) 9152-9159;<https://doi.org/10.1039/C4TA05237D>.
- [31] S. Manzoor, J. Hausele, K. A. Bush, A. F. Palmtrom, J. Carpenter, Z. J. Yu, S. F. Bent, M. D. McGehee, Z. C. Holman, Optics Express, Vol. 26, Issue 21, 21(2018) 27441-27460;  
<https://doi.org/10.1364/OE.26.027441>

- [32] P. Löper, M. Stuckelberger, B. Niesen, J. Werner, M. Filipič, S.-J. Moon, J.H. Yum, M. Topič, S. D. Wolf, C. Ballif, *J. Phys. Chem. Lett.* 6(2015) 66–71; <https://dx.doi.org/10.1021/jz502471h>.
- [33] A. D. Pogrebnjak, A.A. Muhammed, E.T. Karash, N.Y. Jamil, J. Partyk, *Przegląd Elektrotechniczny*, 89(3), (2013) 315-317
- [34] M. Allalla, N. Shukla, S. Minj, S. Tiwari, *Journal of Ravishankar University*, vol 35, Issue 1, (2022); <https://doi.org/10.52228/JRUB.2022-35-1-5>
- [35] F. Azri, A. Meftah, N. Sengouga, A. Meftah, *Solar Energy* 181 (2019) 372–378; <https://doi.org/10.1016/j.solener.2019.02.017>
- [36] T. Bendib, H. Bencherif, M.A. Abdi, F. Meddour, L. Dehimi, M. Chahdi, *Optical Materials*.109 (2020)110259; <https://doi.org/10.1016/j.optmat.2020.110259>.
- [37] E. Karimi, S.M.B. Ghorashi, M. Hashemi, *Journal of optics and photonics (IJOP)* (2014) 57-66
- [38] M.I. Hossain, F.H. Alharbi, N. Tabet, *Solar Energy* 120 (2015) 370–380; <https://doi.org/10.1016/j.solener.2015.07.040>
- [39] T. Minemoto, M. Murata, *J. Appl. Phys.* 116 (2014) 054505; <https://doi.org/10.1063/1.4891982>
- [40] I. M. D. L. Santosa, H. J. Cortina-Marreroa, M.A. Ruíz-Sánchez, L. Hechavarría-Difura, F.J. Sánchez-Rodríguez, M. Courel, H. Hud, *Solar Energy* 199 (2020) 198–205; <https://doi.org/10.1016/j.solener.2020.02.026>
- [41] W. Zhang, Y.C. Wang, X. Li, C. Song, L. Wan, K. Usman, J. Fang, *Adv. Sci.* 5(2018) 1800159; <https://doi.org/10.1002/advs.201800159>
- [42] W. Nie, H. Tsai, R. Asadpour, J.C. Blancon, A. J. Neukirch, G. Gupta, J.J. Crochet, M. Chhowalla, S. Tretiak, M.A. Alam, H.L. Wang, A.D. Mohite, *org science*. 30 (2015) 522-525; <https://doi.org/10.1126/science.aaa0472>.
- [43] S. Rai, B.K. Pandey, D.K. Dwivedi, *Optical Materials*. 100(2020)109631; <https://doi.org/10.1016/j.optmat.2019.109631>
- [44] A. Bag, R. Radhakrishnan, R. Nekovei, R. Jeyakumar, *Solar Energy* 196 (2020) 177–182; <https://doi.org/10.1016/j.solener.2019.12.014>
- [45] D. Liu, M.K. Gangishetty, T.L. Kelly, *J. Mater. Chem. A*, 2(2014) 19873–1988; <https://doi.org/10.1039/C4TA02637C>
- [46] K. Tan, P. Lin, G. Wang, Y. Liu, Z. Xu, Y. Lin, *Solid-State Electronics*, Vol 126, December 2016, Pages 75-80. <http://dx.doi.org/10.1016/j.sse.2016.09.012>.
- [47] L. M. P. Outón, T. P. Xiao, E. Yablonovitch, *J. Phys. Chem. Lett.* 9 (2018) 1703–171; <https://doi.org/10.1021/acs.jpcclett.7b03054>
- [48] P.W. Liang, C.C. Chueh, S. T. Williams, A.K.Y. Jen, *Adv. Energy Mater.* (2015) 1402321; <https://doi.org/10.1002/aenm.201402321>.
- [49] S. Ma, W. Qiao, T. Cheng, B. Zhang, J. Yao, A. Alsaedi, T. Hayat, Y. Ding, Z. Tan, S. Yuan, *Dai ACS Applied Materials & Interfaces*. (2018) 3902–3911; <https://doi.org/10.1021/acsami.7b19053>.
- [50] F. Behrouznejad, a S. Shahbazi, b N. Taghavinia, ac Hui-Ping Wud, E. Wei-Guang Diau, *J. Mater. Chem.* 4(2016)13488; <https://doi.org/10.1039/C6TA05938D>
- [51] M.S. Shamna, K.S. Nithya, K.S. Sudheer, *Mater. Today*(2020)2214-7853; <https://doi.org/10.1016/j.matpr.2020.03.488>
- [52] S. Shao, M. A. Loi, *Adv. Mater. Interfaces*, 7(2020) 1901469 ; <https://doi.org/10.1002/admi.201901469>
- [53] Y. Zhou, Angus G. Weale, *Phys. Chem. Phys.* 18(2016) 4476-4486; <https://doi.org/10.1039/C5CP05371D>
- [54] N. Devi, Khursheed, A. Parrey, A. Aziz, *J. Vacuum Science & Technology. B* 36(2018) 04G105; <https://doi.org/10.1116/1.5026163>
- [55] Y. Wang, Z. Xia, J. Liang, X. Wang, Y. Liu, C. Liu, S. Zhang, H. Zhou, *Semicond. Sci. Technol.* 30 (2015) 054004 ; <https://doi.org/10.1088/0268-1242/30/5/054004>
- [56] X. Wang, X. Zou, J. Zhu, C. Zhang, J. Cheng, Z. Zhou, H. Ren, Y. Wang, X. Li, B. Ren, K. Song, *Materials* 14(2021) 2191 ; <https://doi.org/10.3390/ma14092191>
- [57] Y. Gan, X. Bi, Y. Liu, B. Qin, Q. Li, Q. Jiang, Pei Mo, *J. Energies* 13(2020) 5907 ; <https://doi.org/10.3390/en13225907>

[58] S. Raghvendra, C.Pathak, S. K. Pandey, IEEE Transactions on Electronics Devices,7(2020)67

[59] S. Huang, Z. Rui, D. Chi, and D. Bao, Journal of Semiconductors (2019) 40, 032201;  
<https://doi.org/10.1088/1674-4926/40/3/032201>

[60] S. Huang, Z. Rui, D. Chi, and D. Bao, Journal of Semiconductors (2019) 40, 032201;  
<https://doi.org/10.1088/1674-4926/40/3/032201>